Comparing geometrical and wave optical algorithms of a novel propagation code applied to the VLTI

Rainer Wilhelm[¶]
European Southern Observatory (ESO), Garching b. München, Germany

ABSTRACT

Time-dependent modeling of controlled opto-mechanical systems (e.g. astronomical telescopes) is part of the VLTI system engineering work at ESO. For creation of optical models to be integrated within a dynamic Matlab/Simulink® simulation, a novel optical modeling tool has been developed. It offers a versatile set of geometrical and wave optical propagation algorithms each with its specific strengths. The article describes the algorithms —both from a theoretical and practical point of view. The VLTI as a "real world" application example is presented.

Keywords: geometrical optics, ray tracing, physical optics, wave propagation, beam decomposition, Gaussian beam, stellar interferometry, Very Large Telescope Interferometer

1. INTRODUCTION

Within the scope of the Very Large Telescope Interferometer (VLTI) project, ESO is developing a software package for "integrated modeling" of single- and multi-aperture (quasi-)optical telescopes.[†, 11] Integrated modeling is aiming at time-dependent system analysis combining different technical disciplines (optics, mechanical structure, control system with sensors and actuators, environmental disturbances). Examples of its application are feasibility assessment, performance prediction or reverse engineering for error tracking.

For implementation of dynamic control system simulations, Matlab/Simulink® has been chosen as baseline. All subsystem models will be integrated into this environment. The "**Integrated Modeling Toolbox**" is formed by a set of software modules —each being responsible for model creation of a given subsystem (e.g. optics, structure). Presently, the two most advanced modules of the toolbox are the Structural Modeling Interface "**SMI**" and the optical modeling tool "**BeamWarrior**". Developed in collaboration with the Institute of Light Weight Structures, Technical University of Munich, the Matlab®-based **SMI** provides an interface to the commercial Finite Elements Modeling (FEM) software ANSYS®. It enables the evaluation and creation of condensed structural models to be integrated into the Simulink® environment. **BeamWarrior** is used to generate models of the optical signal flow influenced by perturbations. Its development has been initiated in February 1997 driven by the non-availability of a powerful, open-architecture optical modeling code which can be customized to create optical models for integration into a dynamic control loop simulation. The institutions that have supported this work are Astrium GmbH, Germany, German Aerospace Center (DLR) and ESO. Present and future development is done in joint effort by Astrium GmbH and ESO. The European Space Agency (ESA) is considering **BeamWarrior** as a basis for their planned effort on an integrated model of the infrared space interferometer "DARWIN". For performance and cross-platform portability reasons, the code is written in ANSI C extended by a graphical postprocessor in Matlab®. This article focuses on the beam propagation algorithms. The overall architecture and a description of other features including the creation of optical models for export to Simulink® can be found in other publications.[7, 10, 11, 12]

¶ Email: rwilhelm@eso.org, World Wide Web: http://www.eso.org/projects/vlti

† The term "quasi-optical" denotes that the wavelength is very small compared with the dimensions of the optical surfaces, i.e. the propagating beams have properties resembling those of light waves.

The following Section 2 describes the algorithms for light propagation. Section 3 discusses the algorithms with their individual advantages and drawbacks with regard to their application in practice. A short paragraph addresses the validation of the algorithms. Section 4 shows the application to the VLTI as a "real-world" example. The article ends with a summary and an outlook to future work in Section 5.

2. THEORETICAL DESCRIPTION OF THE PROPAGATION ALGORITHMS

The assumption of a lossless, isotropic and homogeneous medium (refractive index n) is common to all propagation algorithms. For a given medium wavelength $\lambda = \lambda_0/n$, the task is to compute solutions of the scalar *Helmholtz wave equation*

$$(\Delta + k^2)\underline{E}_q(\mathbf{r}) = 0 \tag{1}$$

in form of scalar complex amplitudes $\underline{E}_q(\mathbf{r})$ (q = x, y, z) representing the three Cartesian components of the electric vector field. The medium propagation constant k is defined as $k = 2\pi/\lambda$.

2.1 Geometrical optical propagation algorithm

Geometrical optics (GO) considers the limiting case $\lambda \to 0$. The electric vector field locally[¶] behaves as a homogeneous plane transverse electromagnetic (TEM) wave. Substituting the "trial" solution $\underline{E}_q(\mathbf{r}) = \hat{\underline{E}}_q(\mathbf{r}) \cdot \exp(-jk_0 \cdot \Im(\mathbf{r}))$ into the Helmholtz equation and regarding the case $\lambda \to 0$ one obtains the *eikonal equation* $(\nabla\Im(\mathbf{r}))^2 = n^2$. The scalar function ("eikonal") $\Im(\mathbf{r})$ is a measure of the optical path. The surfaces $\Im(\mathbf{r})$ = constant define GO wavefronts. Light rays are defined as orthogonal trajectories to these wavefronts. In the assumed case of a homogeneous medium a light ray has the form of a straight line. With the unit vector **i** denoting the direction of the light ray, the eikonal can be written as $\Im(\mathbf{r}) = n\mathbf{i} \bullet \mathbf{r}$. The corresponding GO wave signal is

$$\underline{E}_q(\mathbf{r}) = \hat{\underline{E}}_q(\mathbf{r}) \cdot \exp(-jk_0 n\mathbf{i} \bullet \mathbf{r}) = \hat{\underline{E}}_q(\mathbf{r}) \cdot \exp(-j\mathbf{k} \bullet \mathbf{r}) \quad (q = x, y, z). \tag{2}$$

The electric and magnetic field vectors $\underline{\mathbf{E}}$ and $\underline{\mathbf{H}}$ are mutually perpendicular and parallel to the wavefront. Both are perpendicular to the wave vector $\mathbf{k} = k_0 n\mathbf{i}$. $\underline{\mathbf{E}}$ and $\underline{\mathbf{H}}$ share the same phase. The ratio of their magnitudes is the wave impedance $Z = |\underline{\mathbf{E}}|/|\underline{\mathbf{H}}| = Z_0/n$ with the vacuum wave impedance $Z_0 = (\mu_0/\varepsilon_0)^{1/2} \approx 377\Omega$.

A GO beam is modeled by a grid of light rays each having assigned a 2×1 Jones vector $\underline{\mathbf{J}}$. The vector $\underline{\mathbf{J}}$ holds a pair of complex amplitudes $(\underline{E}_{p1}, \underline{E}_{p2})$ with respect to the two local orthogonal polarization directions $\mathbf{p_1}$ and $\mathbf{p_2}$. The three unit vectors $\mathbf{p_1}$, $\mathbf{p_2}$ and **i** form a right-handed orthogonal triad with $\mathbf{p_1} \times \mathbf{p_2} = \mathbf{i}$ (see Figure 1). The amplitude ratio and phase difference of the two components $\underline{E}_{p1}$ and $\underline{E}_{p2}$ determines the local state of polarization. A fast vector-based ray tracing algorithm (Redding & Breckenridge 1991[9]) propagates the ray grid through the optical system consisting of flat, conicoid or cylindrical conicoid surfaces. Each ray is regarded as a sample of a locally plane TEM wave. Therefore, the effect on its Jones vector for reflection or refraction at an optical surface can be described by Fresnel equations. For computing the calibrated power flux through the system, a computationally efficient algorithm has been developed. By using a triangular grid interconnecting the rays (see Figure 1) the approach allows to compute the electric field distribution on a grid of pixels on an optical surface at the expense of a single-forward ray tracing run. For performing the same task, software codes based on stochastic ray tracing require several ray tracing loops from the light source to the target surface. The change in cross-sectional area of a light tube is taken into account for scaling the local squared field amplitude in accordance with the "intensity law of geometrical optics" $I \cdot A$ = constant with the triangle area A and the local intensity $I = 1/(2Z) \cdot |\underline{\mathbf{E}}(\mathbf{r})|^2$. A detailed description of the radiometric polarization ray tracing algorithm can be found in the references.[12, 10]

¶ The term "locally" means "in a region of the spatial extension of some wavelengths.

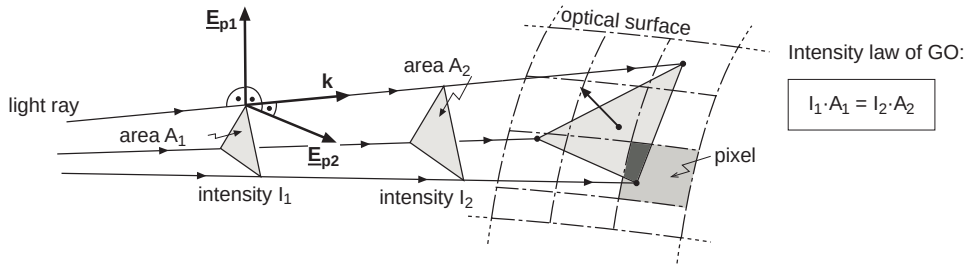

Fig. 1: Triangular ray tubes are used for radiometric scaling of the GO electric field.

2.2 Wave optical propagation algorithms

The limits of validity of the GO model arise from the derivation of the eikonal equation. Practical cases where the GO model is not adequate are the computation of a field distribution close to focus or modeling the propagation of a spatially confined beam over long distances. In these cases, diffraction (i.e. wave optical) effects play an important role. To model such effects, **BeamWarrior** provides a set of different wave optical propagation algorithms which are discussed in the following Subsections 2.2.1, 2.2.2 and 2.2.3. Common to all approaches is their assumption of *scalar diffraction theory*: the coupling of the various vector components of the electric and magnetic field through boundary conditions is neglected. The solution of the Helmholtz equation (Eq. (1)) is computed independently for the three Cartesian components of $\underline{\mathbf{E}}$ resulting in a complete description of the vectorial field. Scalar diffraction theory is an adequate model if (1) apertures are large compared to the wavelength, and (2) a field is not observed too close ($\approx \lambda$) to an aperture.

2.2.1 Direct method

Both, the "direct method" and the "angular spectrum method" (discussed in Subsection 2.2.2) compute the electric field on a "target surface" Σ_t (locations $\mathbf{r_t}$) assuming the knowledge of the electric field on an "object surface" Σ_o (locations $\mathbf{r_o}$). The Helmholtz equation together with the *Kirchhoff boundary condition* for the field on both sides of the aperture on Σ_o and the *Sommerfeld radiation condition* define a boundary value problem.[4] Applying the *Helmholtz–Kirchhoff integral theorem* (derived from *Green's theorem*) with the choice of Sommerfeld's Green's function, one gets the *Rayleigh–Sommerfeld diffraction integral* which forms the base equation of the direct method:

$$\underline{E}_q(\mathbf{r_t}) \;=\; \frac{j}{\lambda}\int_{\Sigma_o}\int \underline{E}_q(\mathbf{r_o}) \cdot \frac{\exp(-jk|\mathbf{r_t}-\mathbf{r_o}|)}{|\mathbf{r_t}-\mathbf{r_o}|} \cdot \mathbf{r_{ot}} \bullet \mathbf{n_o} \cdot dS \qquad (q = x, y, z). \tag{3}$$

For implementation on the computer, the integral in Eq. (3) is replaced by a sum. The field on the target surface is computed as a coherent superposition of spherical wave contributions originating at ray positions $\mathbf{r_o}$ on Σ_o. The approach presumes that the grid of ray triangles is known on the object surface Σ_o. Each ray on Σ_o —with its Jones vector— is interpreted as a *Huygens secondary source*. The spherical wave contributions to a pixel at location $\mathbf{r_t}$ are weighted with an "obliquity factor" $\mathbf{r_{ot}} \bullet \mathbf{n_o}$ where $\mathbf{r_{ot}} = |\mathbf{r_t}-\mathbf{r_o}|^{-1} \cdot (\mathbf{r_t}-\mathbf{r_o})$ is the unit vector pointing from $\mathbf{r_o}$ to $\mathbf{r_t}$, and $\mathbf{n_o}$ is the local unit surface normal at the ray location $\mathbf{r_o}$. The surface element dS (which becomes ΔS_o in the sum) associated to the ray at $\mathbf{r_o}$ is derived from the local ray triangle grid structure around $\mathbf{r_o}$. Figure 2 illustrates the principle of the approach.

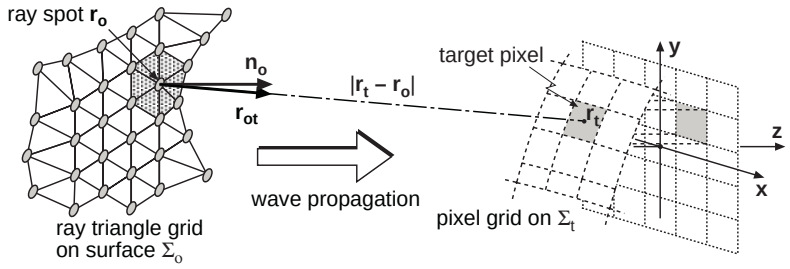

Fig. 2: Principle of the direct method for wave optical propagation

Direct method in paraxial approximation:

The "paraxial approximation" assumes that the field $\underline{E}_q(\mathbf{r}_t)$ can be written as product of a "primary" plane wave propagation factor exp(–jkz) and a wave amplitude $\underline{\Psi}_q(x, y, z)$ whose remaining z-dependence is slow compared to one wavelength and to the transverse variations (along x- and y-direction) due to the finite width of the beam. By dropping the second partial derivative in z, the Helmholtz equation (Eq. (1)) reduces to the paraxial wave equation

$$\frac{\partial^2}{\partial x^2}\underline{\Psi}_q + \frac{\partial^2}{\partial y^2}\underline{\Psi}_q - 2jk\frac{\partial}{\partial z}\underline{\Psi}_q = 0 \qquad (q = x, y, z). \tag{4}$$

Considering the paraxial approximation, the "direct method" solution Eq. (3) becomes

$$\underline{E}_q(x_t, y_t, z_t) = \frac{j}{\lambda z_t} \cdot \exp\left[-jkz_t + \frac{x_t^2 + y_t^2}{2z_t}\right] \cdot \boldsymbol{F}_{2D}\left\{\underline{E}_q(x_o, y_o, 0) \cdot \exp\left[-jk\frac{x_o^2 + y_o^2}{2z_t}\right]\right\} \qquad (q = x, y, z) \tag{5}$$

with the operator $\boldsymbol{F}_{2D}$ denoting a two-dimensional Fourier transform $\{x_o, y_o\} \circ\!\!-\!\!\bullet \{f_x, f_y\}$ defined as follows:

$$\boldsymbol{F}_{2D}\{\Psi(x_o, y_o)\} = \int_{-\infty}^{+\infty}\!\!\int \Psi(x_o, y_o) \cdot \exp[j2\pi(f_x x_o + f_y y_o)]dx_o dy_o. \tag{6}$$

The spatial frequencies $\{f_x, f_y\}$ are defined as $f_x = x_t/(\lambda z_t)$ and $f_y = y_t/(\lambda z_t)$. Eq. (5) assumes that the initial field $\underline{E}_q(x_o, y_o, 0)$ is given on a plane Σ_o parallel to the (x, y)-plane and located at z = 0. The diffracted field $\underline{E}_q(x_t, y_t, z_t)$ is computed on a plane Σ_t parallel to Σ_o at a distance $z = z_t$ ("plane-to-plane propagation"). It is proportional to the Fourier transform of the product of the initial field on Σ_o and a "quadratic phase factor" $\exp[-jk(x_o^2 + y_o^2)/(2z_t)]$.

For computing the Fourier transform, **BeamWarrior** makes use of the FFTW library[¶] —a freely available ANSI C library for computing the Fast Fourier Transform (FFT) in one or more dimensions with arbitrary grid size.

2.2.2 Angular spectrum method

A solution to the boundary value problem mentioned in Subsection 2.2.1 is also obtained by superposing all homogeneous and evanescent plane waves traveling in directions **k** whose complex amplitudes are given by the spatial frequency spectrum ("angular spectrum") of the initial field defined in a plane Σ_o:

$$\underline{E}_q(x_t, y_t, z_t) = \int_{\Sigma_o}\!\!\int \boldsymbol{F}_{2D}\{\underline{E}_q(x_o, y_o, 0)\} \cdot \exp[-j\mathbf{kr}]d\mathbf{k} = \boldsymbol{F}_{2D}^{-1}\{\boldsymbol{F}_{2D}\{\underline{E}_q(x_o, y_o, 0)\} \cdot H(f_x, f_y, z_t)\} \tag{7}$$

¶ The FFTW (Fastest Fourier Transform in the West) library can be downloaded at the URL http://www.fftw.org

with the *transfer function of the homogeneous medium* $H(f_x, f_y, z_t)$ being defined as

$$H(f_x, f_y, z_t) = \exp[-j2\pi\delta \cdot \left|1/\lambda^2 - f_x^2 - f_y^2\right|^{1/2} \cdot z_t] \tag{8}$$

with $\delta = +1$ for $f_x^2 + f_y^2 \le (1/\lambda)^2$ or $\delta = -j$ for $f_x^2 + f_y^2 > (1/\lambda)^2$ (evanescent wave case). As in the paraxial approximation case of the direct approach, Eq. (7) describes a "plane-to-plane propagation" between two parallel planes Σ_o and Σ_t separated by a distance z_t.

Angular spectrum method in paraxial approximation:

In the paraxial case, the transfer function in Eq. (7) reduces to

$$H(f_x, f_y, z_t) = \exp[-jkz] \cdot \exp[j\pi\lambda z_t \cdot (f_x^2 + f_y^2)]\,. \tag{9}$$

2.2.3 Gaussian beam decomposition method

The "Gaussian beam decomposition method" has been invented by A. W. Greynolds[5,6], based on ideas of J. A. Arnaud[1]. In contrast to the two "classical" approaches described above, this powerful alternative technique allows to compute a pure wave optical propagation in an "end-to-end" way —without the need for intermediate geometrical optical propagations. The basic idea of the algorithm is to decompose a field distribution at an aperture into a set of spatially confined "fundamental beams". For calculating the field pattern on any surface of the optical system, the fundamental beams are propagated —including self-diffraction effects— to the surface where they are superposed. The fundamental beam type used in **BeamWarrior** is an astigmatic Gaussian TEM_{00} beam which represents a solution of the paraxial Helmholtz equation (Eq. (4)). Its propagation can be modeled by ray tracing of five rays. The "base ray" defines the main direction of propagation, i.e. the optical axis of the Gaussian beam to which a Jones vector is attached. Four "parabasal" rays (two "waist rays" and two "divergence rays") grouped around the base ray define the self-diffraction of the beam. Figure 3 illustrates the ray-representation of a Gaussian beam whose propagation starts at its beam waist.

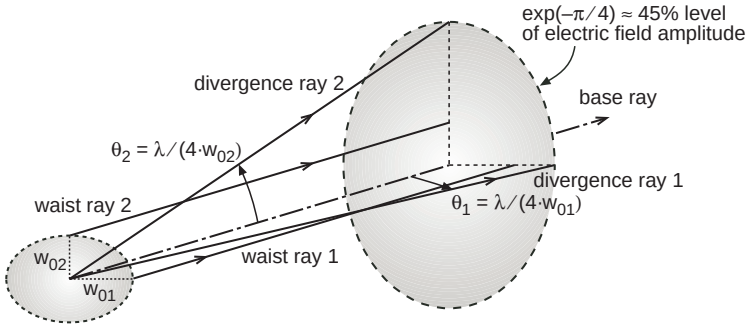

Fig. 3: Representation of an astigmatic Gaussian beam by a base ray and four accompanying parabasal rays. For illustration, the divergence angles are exaggerated.

The *propagation of an arbitrary optical field* is simulated by decomposing the field into a coherent superposition of equidistantly spaced rotationally symmetric Gaussian beams (waist radii $w_{01} = w_{02} = w_0$ in Figure 3) starting their propagation at their beam waists. For each fundamental beam the four parabasal rays are set up in two orthogonal "astigmatic planes" each holding a waist ray and a divergence ray. The initial divergence angles $\theta_1 = \theta_2 = \text{atan}(\lambda/(4{\cdot}w_0))$ are determined by the waist radius w_0. The divergence angle must be small enough, i.e. the initial waist w_0 wide enough, to ensure the validity of the paraxial approximation. The waist should be at least 100 wavelengths wide (e.g. $\lambda = 2\ \mu m \rightarrow w_0 \ge 0.2$ mm). Assuming a minimum number of 10 fundamental beams along one dimension

the spatial extension of the field region to be decomposed has to exceed a minimum value of ~1000·λ. However, there exists an alternative way of decomposing a field distribution which is also applicable for spatial extensions below the above mentioned limit: instead of performing the decomposition in the spatial domain it is carried out in the angular spatial frequency domain. A narrow field region is synthesized by a discrete number of fundamental Gaussian beams propagating in different directions, the waist of each beam being wider than the field region to decompose ("directional decomposition"). We intend to add this decomposition technique in a future release of **BeamWarrior**. It is of practical importance when simulating diffraction at narrow pinholes or optical fiber heads.

Each fundamental beam is propagated by tracing its base ray and the four accompanying parabasal rays using the ray tracing algorithm described in Subsection 2.1. Reflection or refraction at optical surfaces is modeled by reflecting or refracting the beam-constituting rays. As a consequence of the ray-based description of the Gaussian beam it has to be made sure that the region of an optical surface sampled by a single beam is locally parabolic or flat. Within the paraxial approximation each beam has a small self-divergence. The angular deviation of its wavefront from a plane is always quite small. Hence, the distinction between the normal to the wavefront and the base ray direction is not significant. The longitudinal component of the electric field vector is negligible. The local Poynting vector direction is equal to the base ray direction. Since the wavefront of each fundamental beam can be considered as plane, the interaction with a reflecting / refracting optical surface can be modeled by applying Fresnel equations, i.e. the Jones formalism used in the polarization ray tracing (Subsection 2.1) can be used.

The field pattern on an arbitrary surface can be computed from the positions and directions of the base and parabasal rays of the complete set of fundamental beams. Mathematically, each pair of a waist ray and divergence ray is expressed as a complex ray. Complex 2×1 ray vectors are defined in a local transversal coordinate system {X, Y} perpendicular to the base ray (compare Figure 4):

- Complex ray position vectors: $\mathbf{p_k} = \mathbf{p_{D,k}} + j \cdot \mathbf{p_{W,k}}$ (k = 1, 2 for the two astigmatic planes)
- Complex ray direction vectors: $\mathbf{i_k} = \mathbf{i_{D,k}} + j \cdot \mathbf{i_{W,k}}$ (k = 1, 2 for the two astigmatic planes)

where the subscripts "D" and "W" denote divergence and waist ray, respectively. For each pixel on the target surface Σ_t the positions $\mathbf{p_k}$ and directions $\mathbf{i_k}$ are computed in a plane perpendicular to the base ray which contains the pixel. The contribution of a single Gaussian beam to the electric field at the location $\mathbf{r_{loc}} = (X_{pix}, Y_{pix})$ is given by

$$\underline{E}_q(\mathbf{r_{loc}}) = C \cdot \frac{\underline{E}_q(0,0)}{((\mathbf{p_1} \times \mathbf{p_2})_Z)^{1/2}} \cdot \exp[-jkL] \cdot \exp\left[-\pi \frac{\left|(\mathbf{p_1} \times \mathbf{r_{loc}})_Z\right|^2 + \left|(\mathbf{p_2} \times \mathbf{r_{loc}})_Z\right|^2}{4\left|(\mathbf{p_1} \times \mathbf{p_2})_Z\right|^2}\right] \cdot \exp\left[-jk \cdot \mathrm{Re}\left\{\frac{(\mathbf{p_1} \times \mathbf{r_{loc}})_Z(\mathbf{i_2} \bullet \mathbf{r_{loc}}) - (\mathbf{p}_2 \times \mathbf{r_{loc}})_Z(\mathbf{i_1} \bullet \mathbf{r_{loc}})}{2(\mathbf{p_1} \times \mathbf{p_2})_Z}\right\}\right] \tag{10}$$

where L is the distance travelled by the beam and $(\mathbf{a} \times \mathbf{b})_Z$ denotes a two-dimensional vector product whose result is a scalar value $(\mathbf{a} \times \mathbf{b})_Z = a_X b_Y - a_Y b_X$. The real-valued constant C is needed for power calibration.

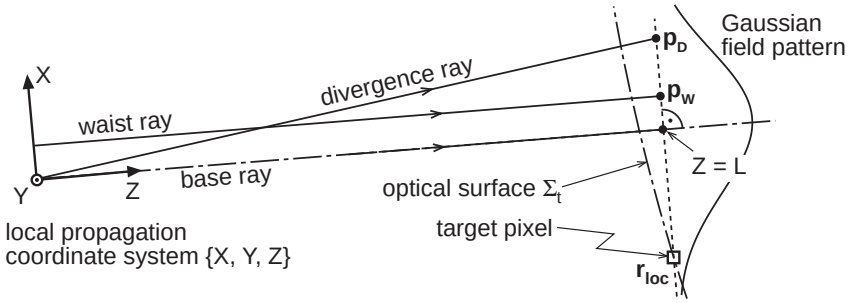

Fig. 4: Contribution of a Gaussian fundamental beam to the electric field on a target pixel (simplified 2D-case)

If the total beam is clipped by an intermediate aperture placed in the beam train a re-decomposition at the aperture may be necessary. In such a case, the sampling rate of the recreated fundamental beams is adjusted to the spatial structures of the obstruction.

3. PRACTICAL CONSIDERATIONS

Following the theoretical description in the previous Section 2, this Section focuses on a more practically oriented summary of pros and cons of the various methods for wave optical propagation.

The ***direct method*** (Subsection 2.2.1) has the disadvantage of relatively long computing times. For a grid of $N \times N$ rays (i.e. Huygens sources) and a $N \times N$ target pixel matrix, the complexity of the algorithm scales as $\sim N^4$. Since the continuous field distribution on Σ_o is sampled at a discrete spatial frequency the calculated diffraction pattern on Σ_t repeats itself in space. Aliasing effects arise in case of too low sampling rates on Σ_o. The method has the advantage to be very accurate except for very small propagation distances. It is applicable to problems with complex and / or skew geometries without requiring a specific coordinate system or the usage of "reference surfaces" to sample the beam. The pixel grid on the target surface Σ_t can be flexibly chosen allowing a high spatial resolution in the computed field. Due to its high accuracy, a typical application is cross-checking a result obtained by another algorithm.

Employing an FFT, the ***direct method in paraxial approximation*** (Subsection 2.2.1) provides a significant increase in computational efficiency. For a pixel grid size of $N \times N$ the algorithm has a complexity of $\sim N^2 \cdot \log_2 N$. As a consequence of the FFT the pixel sizes on object and target surface Σ_o and Σ_t are linked to each other, i.e. they cannot be chosen independently. For a square grid the relation linking the object pixel size Δx_o to the image pixel size Δx_t is: $\Delta x_o \cdot \Delta x_t = \lambda z_t / N$. To improve the spatial resolution on Σ_t columns and lines of zeros are added to the pixel matrix on Σ_o ("zero padding"). Two requirements must be met by the pixel size Δx_o: To avoid aliasing errors in the target field distribution Δx_o has to be small enough to ensure that no significant fraction of the diffracted energy is located at spatial frequencies beyond the maximum value $f_x = 1/(2\Delta x_o)$ captured by the FFT. Second, Δx_o must be small enough to capture phase variations of the field on Σ_o corresponding to one wavelength. For meaningful results there should be at least a few samples per phase change of 2π. A value of 5 samples has proven to be sensible in practice. Therefore it is desirable that the phasefronts of the propagating wave are well aligned to the planes Σ_o and Σ_t. Being more efficient and less flexible than the direct method, this approach is well suited to model the propagation of an almost collimated beam over a large distance.

With and without paraxial approximation the ***angular spectrum method*** (Subsection 2.2.2) has the computational cost of two FFTs, hence a complexity of $\sim 2N^2 \cdot \log_2 N$ for a square $N \times N$ grid. The object and target pixel sizes are equal, $\Delta x_o = \Delta x_t$ which is useful for near-field problems and is a drawback in the far-field case (where one is typically interested in having a large Δx_t and a much smaller Δx_o). Requirements in terms of zero padding and prevention of aliasing are similar to those for the direct method in paraxial approximation. The paraxial approximations of the angular spectrum method (Eq. (7) with Eq. (9)) and the direct method (Eq. (5)) are mathematically equivalent. Both are exact solutions of the paraxial Helmholtz equation (Eq. (4)). However, they differ with respect to their numerical behavior. The oscillating quadratic phase factor in the direct paraxial solution Eq. (5) is proportional to the Fresnel number $N_F = A/\lambda z_t$ leading to a decrease in accuracy for large values of N_F, i.e. in the near-field. In contrast, the transfer function Eq. (9) in the angular spectrum paraxial solution Eq. (7) becomes more oscillatory for small N_F values, hence this solution is less accurate in the far-field. A criterion to decide which method is preferable according to computational efficiency and accuracy has been derived by Mendlovic et al. 1997[8]: A critical distance is given by $z_c = (2A^{1/2} \cdot \delta)/\lambda$ with the initial beam area A (unit m^2) and the object's finest detail δ (unit m). For distances $z < z_c$ the angular spectrum approach should be used whereas for distances $z > z_c$ the direct paraxial method is more adequate.

The ***Gaussian beam decomposition technique*** (Subsection 2.2.3) has many advantages over the "classic" approaches discussed above. Based on tracing rays ("beam tracing") it is the only wave optical algorithm capable of accurately modeling an "end-to-end" propagation through an optical system. Using the direct or angular spectrum methods, such an "end-to-end" propagation is only possible by combining the wave-optical propagations with intermediate geometrical optical propagations within a "hybrid propagation model".[10] The hybrid model allows to reconstruct a ray triangle grid (compare Subsection 2.1) on the basis of an electric field pattern resulting from a diffraction propagation. However, this "mixed" approach does not provide sufficient accuracy for imaging applications with a narrow field-of-view, such as the pupil re-imaging process in the VLTI (field of view 200 arcsec ≈ 1.e–03 rad, see example in Section 4).

Because it does not rely on discrete sampling of the initial field rather than synthesis of the field by continuous fundamental beams, the Gaussian beam decomposition technique does not suffer from aliasing problems. Similar as in the direct method, the target pixel size can be chosen freely. Due to the finite spatial extent of a Gaussian beam the number of pixels on the target surface receiving a significant field contribution is generally lower than the total number of pixels where the field is to be computed. A quick pre-selection of the "illuminated" pixel region for each fundamental beam provides a high computational efficiency, especially in near-field computations. The efficiency inversely scales with the "amount of diffraction" present in the field, i.e. the required time for computing the field pattern at a (intermediate / exit) pupil plane is much shorter than the time required for computing the field pattern at an image plane.

Since for each fundamental beam the integrated optical path is known, temporal coherence effects due to a finite bandwidth $\Delta\lambda << \lambda$ of the radiation can easily be taken into account during field computation. By incoherently combining several spectral bands, a broadband (polychromatic) partial coherent intensity pattern can be computed.

The accuracy of the decomposition technique heavily depends on the sampling quality in the object surface, i.e. the number of fundamental beams, their waist size(s) and the distances between the individual beam centers. Questions and tradeoffs related to the decomposition are discussed in reference[5].

Validation of the modeling concept:

All described algorithms have been extensively validated by different methods. Hereafter, only a short list of the used methods for validation is given:

- Comparison of numerical results (spatial distribution of field amplitude and phase, phase of the spatially averaged field) obtained with different algorithms
- Comparison of numerical results with analytical ones (in cases which can be described by analytical formulae (e.g. diffraction at a circular or rectangular aperture)
- Checking the $\lambda \rightarrow 0$ convergence of wave-optical results towards the geometrical optical result

4. MODELING THE PUPIL RE-IMAGING IN THE VLTI

The VLTI is formed by the coherent combination of the four "VLT Unit Telescopes (UTs)" (diameter 8.2 m) and several movable "Auxiliary Telescopes (ATs)" (diameter 1.8 m).[3] The stellar interferometer array is located on top of Cerro Paranal in the Atacama desert, Chile. While some subsystems are still under construction, the VLTI recorded its "first fringes" on the star Alpha Hydrae in March 2001 using two "test siderostats (SIDs)" (with flat primary mirror, 40 cm diameter) as photon collectors separated by a baseline of 16 m. The diameter of the star was measured to be 0.00929±0.00017 arcsec, i.e. with an error of less than 2 %. The initial observations proved the concept of two core subsystems of the VLTI: (1) the "Delay Lines" which are precisely movable cat's–eye retro-reflectors used to equalize the optical paths in the two (or more) interferometer arms (see Figure 5), and (2) "VINCI", the "VLTI Inter-

ferometer Commissioning Instrument" which performs the coherent beam combination at the near infrared wavelength $\lambda = 2.2$ µm. First fringes with the UTs are planned for end of 2001. Within the following years, additional beam combination instruments operating in different spectral bands will be added. The presence of ATs will enhance the spatial frequency coverage of the array. A dual-feed facility that allows simultaneous observation of two objects will boost the sensitivity by allowing long integration times on faint sources while tracking the fringes of a bright unresolved "reference star".

At ESO the optical modeling tool **BeamWarrior** has been employed to analyze the effects of diffraction on the propagation of the starlight beams and laser beams which are used for high-precision metrology. One important result is the loss of optical energy due to clipping of the starlight beam at the 20 cm Delay Line entrance aperture. The effective propagation distances along the underground light duct and Delay Line tunnel can reach up to 200 m. This causes significant diffractive spreading of the starlight beam with its pupil diameter of 8 cm (UT / SID) (1.8 cm for AT). In addition to the inevitable losses due to beam clipping, diffraction causes the stellar beams in the interferometric laboratory to considerably differ from their geometrical optical footprints leading to difficulties in certain beam combination schemes. This effect can effectively be compensated by actively re-imaging the telescope exit pupil to a fixed location in the beam combination laboratory (see Figure 5). Besides this, the original objective of pupil re-imaging is a wide unvignetted field-of-view. The pupil re-imaging will be performed by two convex spherical field mirrors located in the beam train: (1) the VCM (Variable Curvature Mirror)[2] of the Delay Line Ritchey–Chretien telescope whose curvature can be adjusted using a pressure chamber, and (2) the fixed-curvature field mirror of a beam compressor telescope which reduces the beam diameter of a starlight beam (UT / SID) entering the laboratory from its initial value of 8 cm to 18 mm.

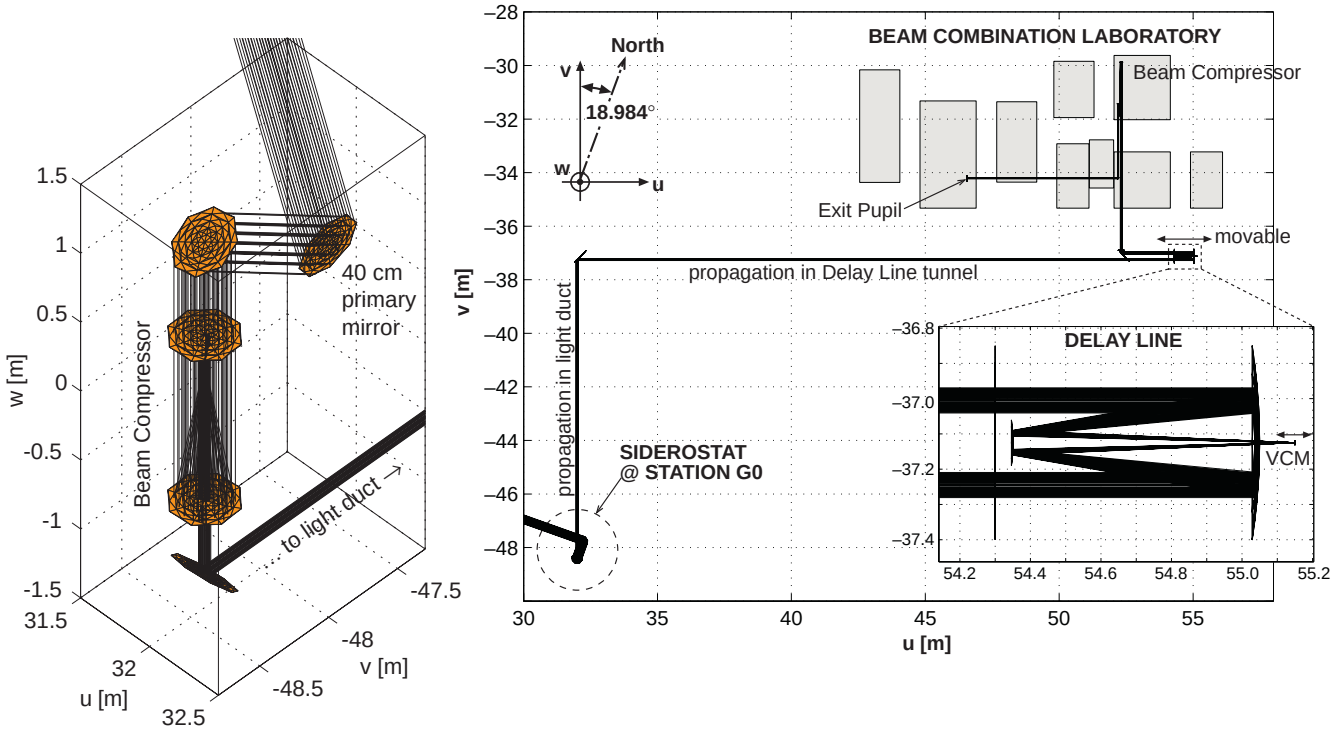

*Fig. 5: Left: Scaled **BeamWarrior** model of a test siderostat; Right: scaled **BeamWarrior** model of the VLT Interferometer arm related to a siderostat at station "G0". The instrument tables in the laboratory are shown.*

In the current commissioning phase a mirror with a fixed radius of curvature of 1 m is taken in place of the VCM. The effect of the resulting incorrect "pupil re-imaging" has been assessed by calculation of an "end-to-end" wave

optical propagation from the sky to the exit pupil in the laboratory assuming two different radii of curvature for the VCM: the current fixed value R_1 = 1 m and a value of R_2 = 2.073 m adjusted to correctly re-image the SID exit pupil located in the SID beam compressor.¶ In this simulation, the section of the incident plane wavefront cut out by the SID primary mirror is decomposed into a set of 4790 paraxial Gaussian beams. Each fundamental beam has a waist radius of 3 mm (≈ 1300 λ). The ratio of the distance between the centers of two adjacent beams versus their waist diameters is 0.75. A pointing towards {altitude, azimuth} = {50°, 270°} has been chosen. The resulting electric field distributions in the nominal exit pupil are shown in Figure 6 (amplitude) and Figure 7 (phase).

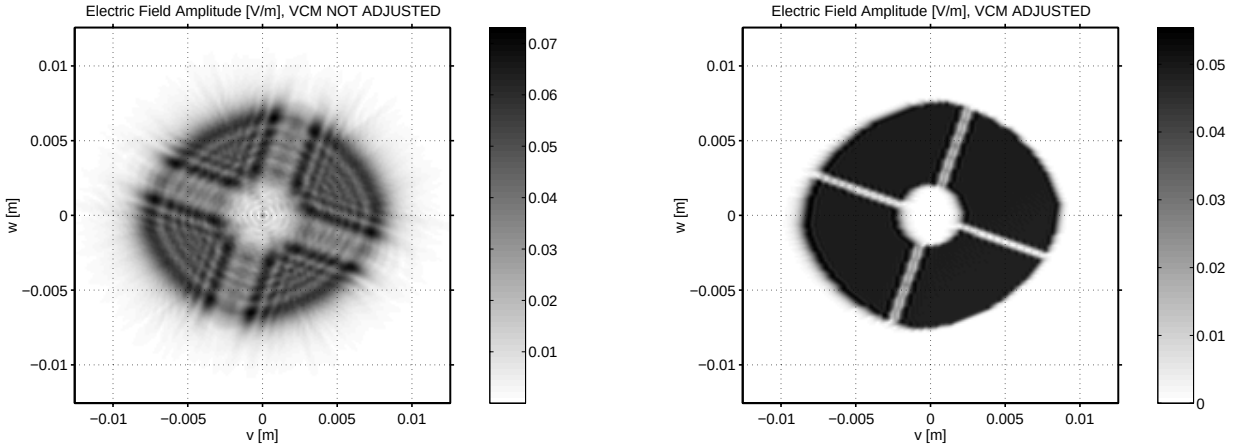

Fig. 6: Electric field amplitude [V/m] (one Cartesian component) at the nominal exit pupil in the beam combination laboratory (see Figure 5) (Siderostat starlight beam, λ = 2.2 μm, Δλ = 200 nm, star magnitude m = –6, Aluminum mirrors); Left: with a VCM radius of curvature of R_1 = 1 m (as in current operation); Right: with a VCM radius of curvature of R_2 = 2.073 m —adjusted to correctly re-image the pupil. The two transversal coordinates v and w refer to the VLTI site coordinate system {u, v, w} as shown in Figure 5.

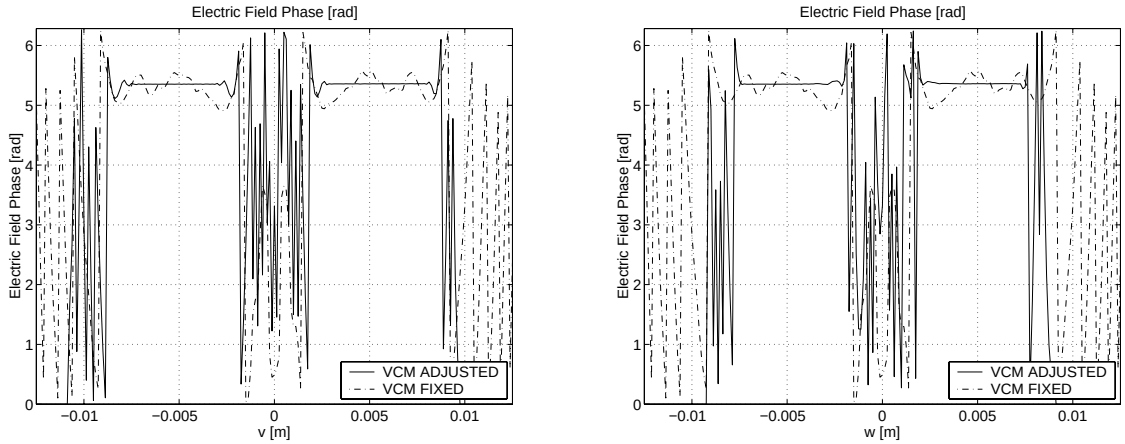

Fig. 7: Electric field phase [rad] (one Cartesian component) at the nominal exit pupil in the beam combination laboratory (see Figure 5) for two different curvatures of the VCM (R_1 = 1 m and R_2 = 2.073 m); The two plots show the phase map drawn in sections along the two transversal directions v and w.

The field pattern corresponding to the fixed VCM radius of curvature R_1 shows clearly noticeable diffraction effects in amplitude and phase. In the VINCI beam combiner the stellar beams are coupled into optical fibers before their

¶ The correct VCM radius of curvature is computed using a paraxial geometrical optics formula.

interferometric combination in an X-coupler. Therefore, the pupils are focused onto fiber heads. A quantity of interest is the coupling efficiency into the fiber which has an impact on the signal-to-noise ratio of the fringe detection process.

The computed intensity pattern of the pupil image focused on a VINCI fiber head is plotted in Figure 8 for the VCM radius of curvature R_1. The differences between the intensity maps obtained for R_1 and R_2 are very small —with a maximum difference of 1.7 % on the optical axis. This means that the diffraction effects visible in the pupil for R_1 will not have a significant influence on the coupling efficiency, i.e. they will not lead to a significant decrease in signal-to-noise ratio.

It is emphasized that the presented example represents one of many possible interferometer geometries of the VLTI. The results strongly depend on the chosen configuration, i.e. telescope location and Delay Line position.

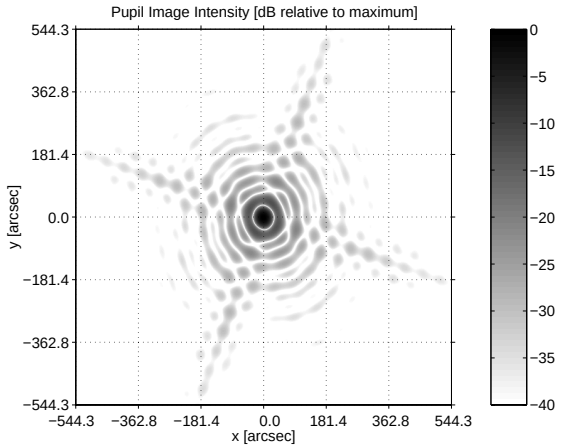

Fig. 8: Intensity [dB relative to maximum] of the pupil image focused on a VINCI fiber head; The first zero occurs at an angle of λ/d = 2.2 µm / 18 mm ≈ 30 arcsec. The image corresponds to the case R_1 = 1 m (incorrect pupil re-imaging). The solution for R_2 = 2.073 m (not shown here) differs only slightly (< 1.7 %) from the R_1 = 1 m case.

5. SUMMARY AND FUTURE WORK

Aiming at the generation of optical models to be integrated into time-dependent simulations of controlled opto-mechanical systems, a novel modeling tool (**BeamWarrior**) has been developed. It is based on a set of different algorithms for modeling light propagation through homogeneous media. The geometrical optical domain is covered by a radiometric polarization ray tracing algorithm. Wave optical (diffraction) propagation is handled by three alternative approaches, each being suitable for specific cases: (1) the direct method based on the Rayleigh–Sommerfeld integral, (2) the angular spectrum method using a decomposition of the optical field into a set of homogeneous and evanescent plane waves, and (3) the powerful Gaussian beam decomposition technique which allows to simulate an "end-to-end" wave optical propagation. All algorithms consider polarization effects and are radiometrically calibrated.

Following a theoretical description of the propagation algorithms, the article summarizes pros and cons of the different methods with regard to their application in practice. The modeling concept is illustrated by showing some results of an analysis which has been performed to assess the effect of diffraction on the pupil re-imaging process in the VLTI. A main future objective is the extension of the Gaussian beam decomposition algorithm towards a "directional decomposition scheme" which is required to model diffraction at fine structures as mentioned in Subsection 2.2.3.

ACKNOWLEDGEMENTS

The author wishes to thank his colleagues from the ESO VLTI Group and Astrium ED for fruitful discussions. Thanks to Alberto Gennai for reviewing the manuscript.

REFERENCES

1. J. A. Arnaud, "Nonorthogonal Optical Waveguides and Resonators", *Bell System Technical Journal*, **Nov. 1970**, p. 2311, 1970
2. M. Ferrari, F. Derie, G. R. Lemaitre, S. Mazzanti, "VLTI Pupil Transfer: Variable Curvature Mirrors — Final Results and Performances, and Interferometric Optical Laboratory Layout", *Interferometry in Optical Astronomy*, P. J. Lena, A. Quirrenbach, Editors, Proc. SPIE Vol. **4006**, Part One, pp. 104–115, 2000
3. A. Glindemann et al., "The VLT Interferometer: a unique instrument for high-resolution astronomy", *Interferometry in Optical Astronomy*, P. J. Léna, A. Quirrenbach, Eds., Proc. SPIE Vol. **4006**, Part One, pp. 2–12, 2000
4. J. W. Goodman, *Introduction to Fourier Optics*, McGraw-Hill Publishing Company, New York, 1968
5. A. Greynolds, "Propagation of general astigmatic Gaussian beams along skew ray paths", *Diffractive Phenomena in Optical Engineering Applications*, Proc. SPIE Vol. **560**, pp. 33–50, 1985
6. A. Greynolds, "Vector-formulation of ray-equivalent method for general Gaussian beam propagation", *Current Developments in Optical Engineering and Diffractive Phenomena*, Proc. SPIE Vol. **679**, pp. 129–133, 1986
7. M. Kersten, A. Weidler, R. Wilhelm, U. Johann, L. Szerdahelyi, "OISI Dynamic End-to-End Modeling Tool", *Interferometry in Optical Astronomy*, P. J. Léna, A. Quirrenbach, Eds., Proc. SPIE Vol. **4006**, Part Two, pp. 881-892, 2000
8. D. Mendlovic, Z. Zalevsky, N. Konforti, "Computation considerations and fast algorithms for calculating the diffraction integral", *Journal of Modern Optics*, Vol. **44**, No. 2, pp. 407–414, 1997
9. D. C. Redding, W. G. Breckenridge, "Optical Modeling for Dynamics and Control Analysis", *Journal of Guidance, Control and Dynamics*, Vol. **14**, No. 5, pp. 1021–1032, 1991
10. R. Wilhelm, U. Johann, "Novel approach to dynamic modeling of active optical instruments", *Design and Engineering of Optical Systems II*, F. Merkle, Ed., Proc. SPIE Vol. **3737**, pp. 45–56, 1999
11. R. Wilhelm, B. Koehler, "Modular toolbox for dynamic simulation of astronomical telescopes and its application to the VLTI", *Interferometry in Optical Astronomy*, P. J. Léna, A. Quirrenbach, Eds., Proc. SPIE Vol. **4006**, Part One, pp. 124–135, 2000
12. R. Wilhelm, *Novel numerical model for dynamic simulation of optical stellar interferometers*, Logos Verlag Berlin, 2000, also: Technische Universität Berlin, Dissertation, 2000